Physica 3D (1981) 627–636
North-Holland Publishing Company

EVOLUTION OF WIGNER'S PHASE-SPACE DENSITY UNDER A NONINTEGRABLE QUANTUM MAP

H.J. KORSCH* and M.V. BERRY†
H.H. Wills Physics Laboratory, Tyndall Avenue, Bristol BS81TL, UK

Received 29 December 1980

A nonintegrable area-preserving map for a system with one freedom is quantized, and the evolution of Wigner's function $W(q,p)$ illustrated by contour plots of W in the phase plane. In the classical limit, propagation is governed by Liouville's equation and the contours of W rapidly develop an intricate structure of whorls and tendrils. When Planck's constant $\hbar$ is not zero, the quantum map smooths out classical detail in phase-space areas smaller than $\hbar$. The quantum-mechanical distributions spread more slowly than their classical counterparts.

1. Introduction

For most Hamiltonians, the classical equations of motion are non-integrable. One consequence of this is chaotic motion, in which initially close orbits can eventually get far apart, and, conversely, initially distant orbits can come close together. In the classical phase space, an initial distribution of points will develop a fantastic complexity of 'whorls' and 'tendrils', as explained by Berry, Balazs, Voros and Tabor [1]. Over long times this classical complexity develops without limit, leading to phase-space distributions with structure on arbitrarily small scales. Quantum-mechanically, however, the uncertainty principle denies meaning to structure in phase-space volumes smaller than $\hbar^N$, where $\hbar$ is Planck's constant and N the number of freedoms. $\hbar$ must therefore act to smooth out the classical fine structure and cause the correspondence principle to break down for long times.

In this paper we illustrate this '$\hbar$-smoothing' of classical complexity by computations for a maximally simple model with one freedom, whose phase space is the plane. Nonintegrability will be introduced by making the Hamiltonian time-dependent, with the time-dependence so chosen that the classical motion can be expressed as an explicit discrete-time map of phase space. As explained in [1] the (local) classical map can be converted into a (nonlocal) 'quantum map' operating on Wigner's phase-space density function [2–7]. The advantage of the Wigner formalism is that the evolution of a statistical mixture of quantum states or of a pure quantum state, can be displayed directly in phase space along with its classical limit, which is a probability density evolving according to Liouville's equation. The pioneering computations of Wigner functions associated with classically chaotic motion were carried out by Hutchinson and Wyatt [13], for stationary states of the Hénon-Heiles system, which has two freedoms, rather than for evolving states of a time-dependent system with one freedom.

2. Phase-space classical and quantum maps for a periodically kicked particle

The Hamiltonian

$$H(q,p,t) = \frac{p^2}{2\mu} + TV(q) \sum_{n=-\infty}^{\infty} \delta(t - nT) \qquad (1)$$

* Permanent address: Fachbereich Physik, Universität Kaiserslautern, D6750 Kaiserslautern, West Germany.
† Present address: Institute for Theoretical Physics, Princetonplein 5, Utrecht, The Netherlands.

0167-2789/81/0000–0000/$02.50

describes a particle of mass μ moving along the line $(-\infty < q < +\infty)$ and being kicked at regular intervals T with an impulse $-T\,\mathrm{d}V(q)/\mathrm{d}q$ that depends on where it is. Hamilton's equations show that if the phase space q,p is illuminated 'stroboscopically' at times t_n separated by T, points q_n,p_n move classically according to the area-preserving map

$$\left.\begin{aligned} q_{n+1} &= q_n + p_n T/\mu \\ p_{n+1} &= p_n - T\,\frac{\mathrm{d}V}{\mathrm{d}q}(q_{n+1}) \end{aligned}\right\}. \tag{2}$$

(A similar map with q representing a cyclic coordinate – the 'kicked rotor' – was studied classically and quantum-mechanically by Casati, Chirikov, Izraelev and Ford [8].)

A phase-space probability distribution $W_n(q,p)$ evolves classically according to

$$W_{n+1}(q,p) = \int_{-\infty}^{\infty} \mathrm{d}q' \int_{-\infty}^{\infty} \mathrm{d}p' K^{\mathrm{cl}}(q,p;q',p') W_n(q,p), \tag{3}$$

where K^{cl} is the classical Liouville propagator

$$K^{\mathrm{cl}}(q,p;q',p') = \delta(q' - q + p'T/\mu)\delta(p - p' + TV'(q)). \tag{4}$$

Under this propagation, a closed contour of W_n preserves its area as each of its points maps according to (2). But as n (i.e. t) increases, then, as described in [1], the contours of W_n get longer and increase in complexity by the formation of 'whorls' and 'tendrils' associated with the fixed points of (2).

The nonintegrability of (2) is described by the discretization parameter T. As $T \to 0$, the Hamiltonian (1) corresponds to motion in the stationary potential $V(q)$, which is integrable. If $V(q)$ is constant, linear, or quadratic, (2) is integrable for any T. The simplest potential corresponding to bound motion when $T = 0$ and giving a non-integrable map when $T \neq 0$ is

$$V(q) = Aq^4/4, \tag{5}$$

which under the scaling

$$x \equiv qT\sqrt{\frac{A}{\mu}}, \quad y \equiv p\,\frac{T^2}{\mu^{3/2}}\sqrt{A} \tag{6}$$

gives the parameter-free 'quartic map'

$$\left.\begin{aligned} x_{n+1} &= x_n + y_n \\ y_{n+1} &= y_n - x_{n+1}^3 \end{aligned}\right\}. \tag{7}$$

This is the case for which the calculations described in the next section are carried out.

Quantum-mechanically, we shall study the evolution of Wigner's function $W(q,p)$, defined as follows [2–7]: Let the system be described by a density matrix $\hat{\rho}$ corresponding to a mixture of states $|\psi_j\rangle$ with probabilities a_j, i.e.

$$\hat{\rho} = \sum_j a_j |\psi_j\rangle\langle\psi_j| \quad \left(a_j \geq 0, \sum_j a_j = 1\right). \tag{8}$$

Then

$$W(q,p) \equiv \frac{2\pi}{h^2}\,\mathrm{Tr}\left[\hat{\rho} \int_{-\infty}^{\infty} \mathrm{d}Q \int_{-\infty}^{\infty} \mathrm{d}\Pi \exp\left\{\frac{\mathrm{i}}{\hbar}(\hat{p} - p)Q + (\hat{q} - q)\Pi\right\}\right], \tag{9}$$

where $\hat{q}$ and $\hat{p}$ are the position and momentum operators. This definition implies [6] that W is real, and that

$$\int_{-\infty}^{\infty} \mathrm{d}q \int_{-\infty}^{\infty} \mathrm{d}p W(q,p) = 1 \tag{10}$$

and

$$\int_{-\infty}^{\infty} \mathrm{d}q \int_{-\infty}^{\infty} \mathrm{d}p W^2(q,p) \leq \frac{1}{h}, \tag{11}$$

the equality sign holding if $\hat{\rho}$ corresponds to a pure state, i.e. if $a_j = \delta_{jk}$ in some representation.

The evolution of W is governed by the quantum map derived from (1) by replacing q and p by $\hat{q}$ and $\hat{p}$. As shown in [1], this map is

$$W_{n+1}(q,p) = \int_{-\infty}^{\infty} \mathrm{d}q' \int_{-\infty}^{\infty} \mathrm{d}p' K(q,p;q',p') W_n(q,p), \tag{12}$$

where K is the Wigner propagator

$$K(q,p;q',p') = \frac{2}{\hbar}\,\delta\left(q' - q + p'\frac{T}{\mu}\right) \times \int_{-\infty}^{\infty} \mathrm{d}\xi \exp\left\{\frac{\mathrm{i}}{\hbar}[2\xi(p'-p) - T\{V(q+\xi) - V(q-\xi)\}]\right\}. \tag{13}$$

This shows that points map locally in position but non-locally in momentum. When $\hbar = 0$, K reduces to K^{cl}, given by (4), and the map becomes local in both variables.

For the quartic potential (5), we use the scaling (6) and the following additional scaling of Planck's constant:

$$\hbar' \equiv \hbar A T^3/\mu^2. \tag{14}$$

The integral in (13) can be evaluated exactly in terms of the Airy function [9], and the quantum map (12) becomes

$$W_{n+1}(x,y) = \frac{2}{(\hbar')^{2/3}|6x|^{1/3}} \times \int_{-\infty}^{\infty} \mathrm{d}x'\, \mathrm{Ai}\left\{\frac{-2\,\mathrm{sign}(x)}{(\hbar')^{2/3}|6x|^{1/3}}(x - x' - y - x^3)\right\} \times W_n(x', x - x'). \tag{15}$$

Despite appearances, there is no singularity at $x = 0$, and a smooth W_n generates a smooth W_{n+1}.

In both the classical and the quantum-mechanical cases we shall study the iteration of an initial density $W_0(x,y)$ which is a Gaussian packet centred on $\bar{x}$ and $\bar{y}$ with variance Δ^2 in x and y, i.e.

$$W_0(x,y) = \frac{1}{2\pi\Delta^2} \exp\left\{-\frac{1}{2\Delta^2}[(x-\bar{x})^2 + (y-\bar{y})^2]\right\}. \tag{16}$$

In order to represent a quantum-mechanical mixed state, this must satisfy the inequality (11), leading to the condition

$$\Delta^2 \geqslant \hbar'/2 \tag{17}$$

– obviously an expression of the uncertainty principle.

The first iteration of a Gaussian W_0 under the quantum map (15) can be carried out analytically, with the result

$$W_1(x,y) = \frac{\lambda}{2\Delta\sqrt{\pi}} \exp\left\{-\left(\frac{u}{\lambda\Delta}\right)^2 + \frac{2}{3}(\lambda\Delta)^6 - \frac{\lambda^2\Delta^2 v}{2}\right\} \mathrm{Ai}\left\{-v + \left(\frac{\lambda\Delta}{2}\right)^4\right\}, \tag{18}$$

where

$$\lambda \equiv \frac{2\,\mathrm{sign}(x)}{(\hbar')^{2/3}|6x|^{1/3}},$$
$$u \equiv \frac{\lambda}{2}(x - \bar{x} - \bar{y}), \tag{19}$$
$$v \equiv \frac{\lambda}{2}(x - 2y - 2x^3 - \bar{x} + \bar{y}).$$

This is an instructive result, because it shows that even after one iteration Wigner's function takes on negative values (in parts of the region where the Airy function has negative argument), emphasising the fact that W is an essentially quantum-mechanical object which is not a probability density [2–5]. A short calculation shows that because of the exponential factor in (18) these negative values are very small in

magnitude, and that as $\hbar' \to 0$ the regions where they occur recede to infinity, leaving a classically iterated W which is always positive, as it should be.

Further iterations of the quantum map were carried out numerically, with results described in the next section.

3. Computations of Wigner's function

The results of mapping the initial Gaussian Wigner function $W_0(x,y)$, given by (16), are most conveniently displayed in both the classical and quantum-mechanical cases as contour maps of the iterates $W_n(x,y)$ in the xy plane. Classically, points on the contours were mapped by (7). Quantum-mechanically, the integral in (15) was evaluated on a grid of points x and y (typically 10^4 points in the square $|x| < 2$, $|y| < 2$) and contours of W_n plotted by interpolating between the grid points; the squares drawn on these contour maps have area equal to the value of $\hbar'$ employed in their calculation.

Fig. 1 shows five iterations of the classical map, starting from a Gaussian centred on the origin ($\bar{x} = \bar{y} = 0$) and with width $\Delta = 0.5$. The central contours can be seen to curl into 'whorls' around the origin where the map (7) has an elliptic fixed point (cf. fig. 9 of [1]). The outer contours send thin 'tendrils' flailing outwards as their points escape chaotically. This escape is very fast: according to (7), points in the outer region recede as $\exp(3^n)$, behaviour originally revealed by computation (P. Richens, private communication).

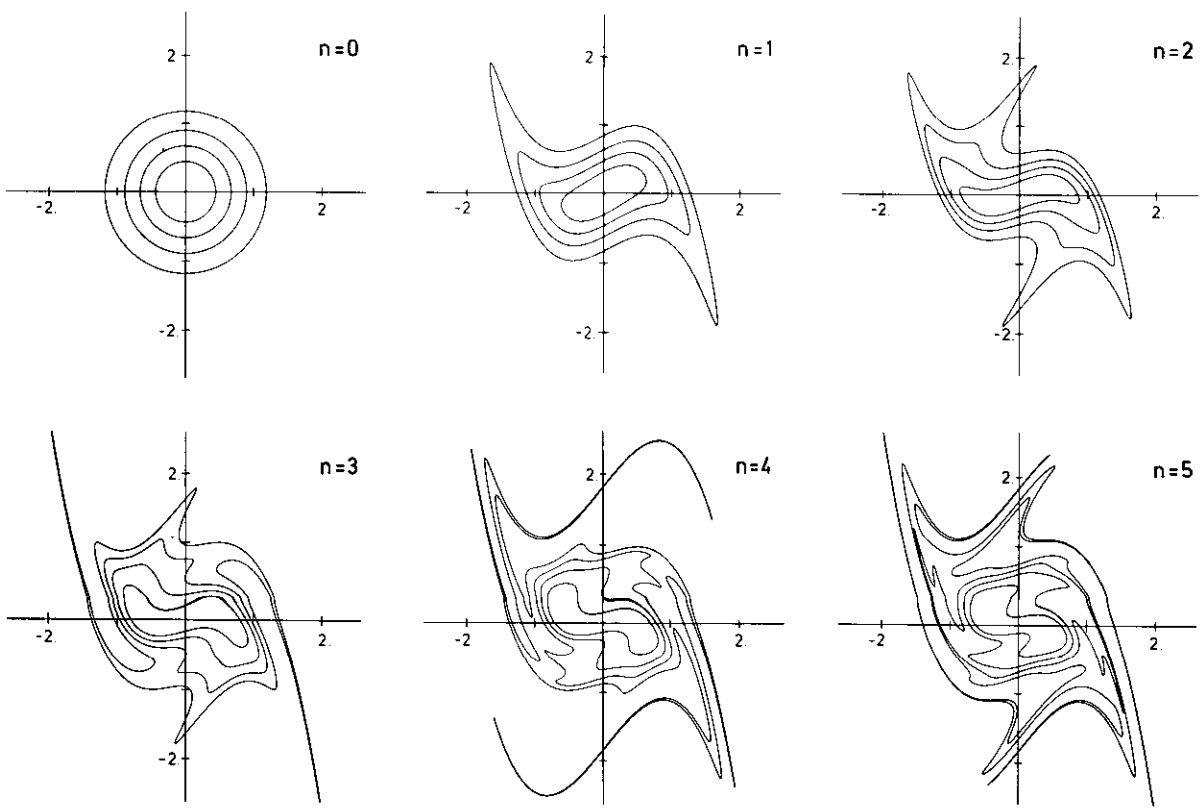

Fig. 1. Classical mapping of an initial Gaussian phase-space density $\exp\{-(x^2+y^2)/2\Delta^2\}$ with $\Delta = 0.5$ for $n = 0,1,2,3,4,5$. The contour lines are drawn for 80%, 60%, 40% and 20% of the maximum of the initial distribution.

Fig. 5 shows five iterations of the classical map, starting from a displaced Gaussian ($\bar{x} = 0.78$, $\bar{y} = 0$) with width $\Delta = 0.25$. This lies largely in the chaotic region of the map, and quickly sends a tendril out towards infinity.

Now we display the quantum maps. Fig. 2 begins with the same Gaussian $W_0(x,y)$ as fig. 1, but now $\hbar' = 0.1$ instead of zero. The effect of finite $\hbar'$ is clearly to inhibit the development of fine detail. This can first be seen on the maps for $n = 2$, where the sharpest part of the outer contour in fig. 1 is slightly smoothed on fig. 2. The thin tendrils that appear classically when $n \geq 3$ are completely absent from fig. 2.

Fig. 3 is the same as fig. 2 except that $\hbar'$ takes the extreme quantum value permitted by (17), namely $\hbar' = 0.5$, corresponding to a Gaussian-packet pure state. The inhibition of fine structure is more marked than in fig. 2 and is evident even for $n = 1$. Between $n = 1$ and $n = 5$ this quantum-mechanical Wigner function changes little, whereas the classical function develops the intricate structure shown in fig. 1. In particular, the quantum-mechanical function remains compact (at least to the contour levels shown) while the classical function explores an increasing area of the plane.

Fig. 4 shows the first three iterations of the same initial Gaussian, for a series of values of $\hbar'$ decreasing from the maximum possible value of 0.5 to the classical value of zero. The maps for $n = 3$ show particularly clearly how the classical fine detail is progressively revealed as $\hbar'$ gets smaller. It appears that the most obvious effect of quantum mechanics is indeed what one would expect, namely to obliterate classical detail on areas smaller than $\hbar'$.

Finally fig. 6 shows the first five mappings of

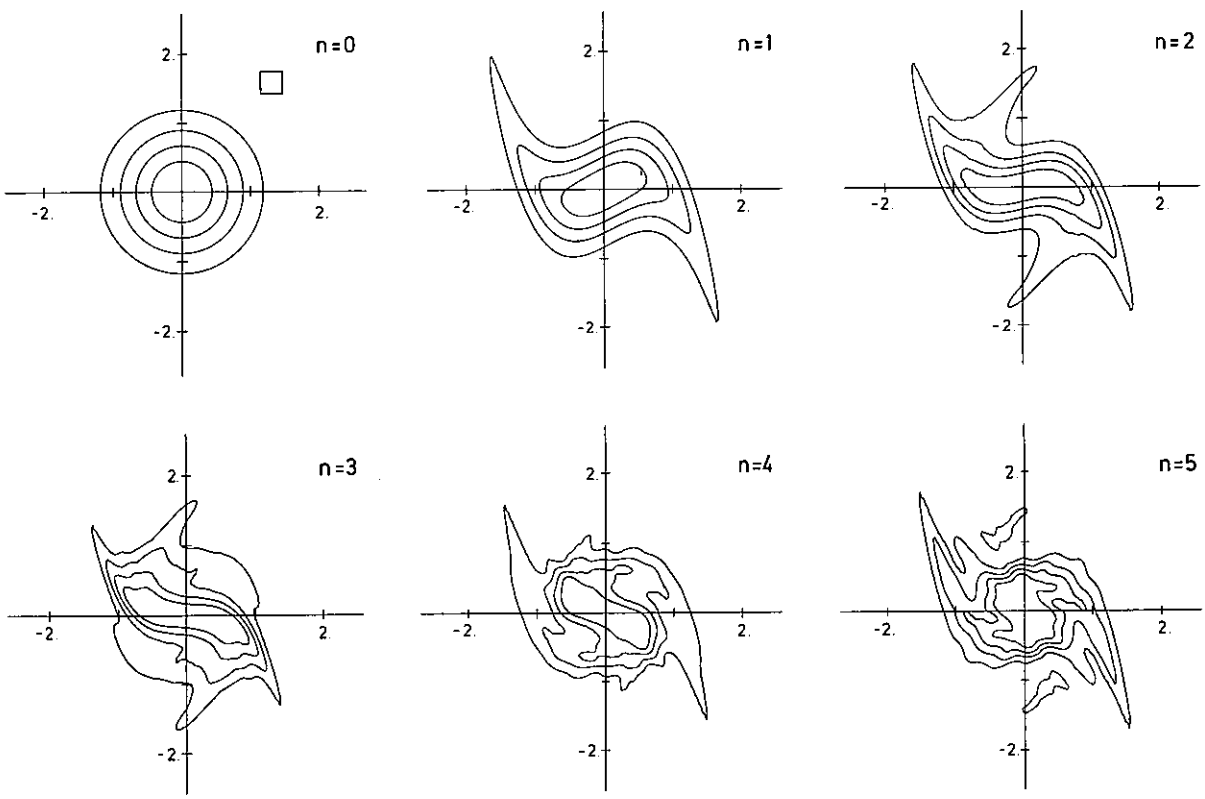

Fig. 2. Quantum mapping of the Wigner density $W_n(x,y)$ for $n = 0,1,2,3,4,5$. The initial distribution and contours are the same as in fig. 1. $\hbar' = 0.1$ and a square of this area is drawn on the $n = 0$ picture.

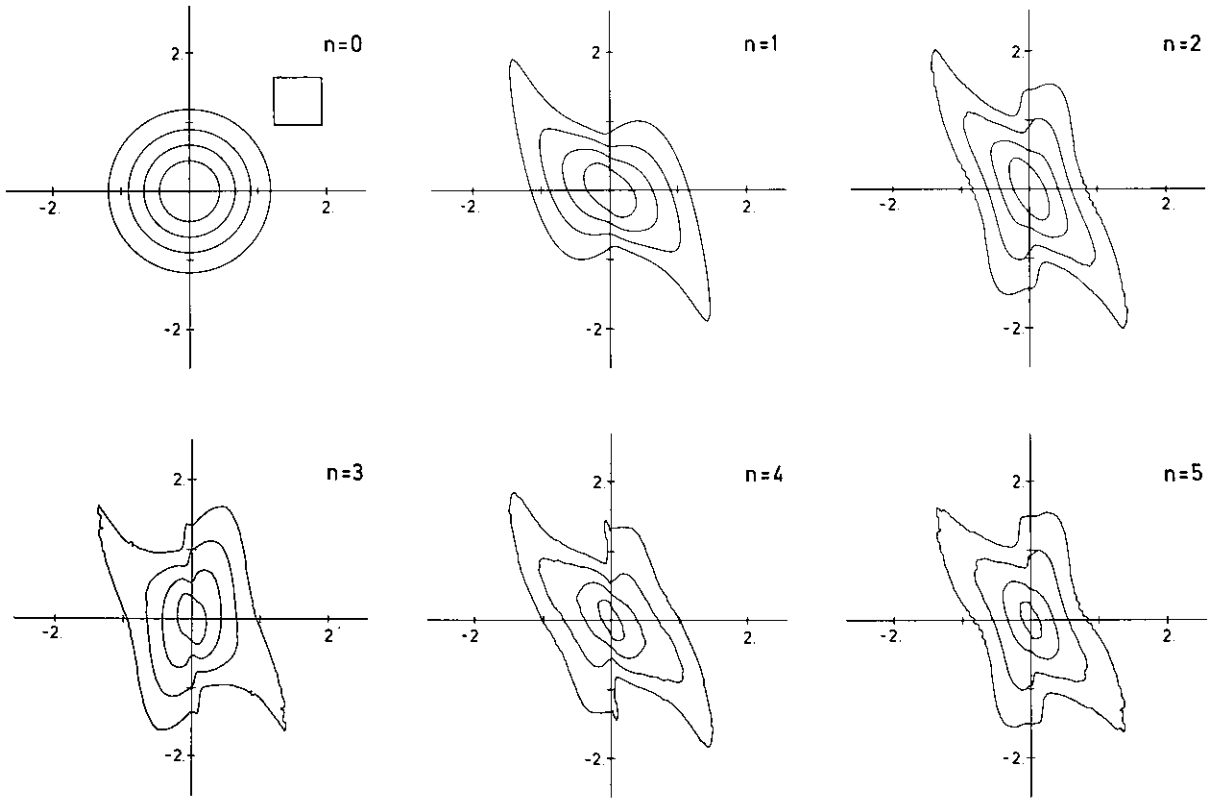

Fig. 3. As fig. 2 but with $\hbar' = 0.5$ (extreme quantum-mechanical case).

the same displaced initial Gaussian as in fig. 5, but with $\hbar'$ equal to its largest possible value, namely 1/8. The point of maximum probability follows approximately the corresponding point of the classical distribution, but there are significant deviations. The most striking difference, however, is the complete absence in fig. 6 of the long tendril in fig. 5; instead, the quantum-mechanical packet remains quite compactly distributed.

4. Discussion

Usually, the effect of a nonzero value of Planck's constant $\hbar$ is to superimpose quantum detail onto a smooth classical background (a striking example is the intricate pattern of interference fringes [10] decorating caustic singularities of families of trajectories). But our computations show $\hbar$ having the opposite effect, of smoothing away fine detail that the classical path structure develops over long times.

Now we discuss the spreading of the distribution under the map. In quantum-mechanics textbooks, spreading is usually illustrated with the example of a Gaussian packet moving freely. In fact in this case the dynamics of the spreading is purely classical, because when $V(q) = 0$ the propagator (13) reduces to the Liouville form (4). Quantum-mechanics enters only in the choice of initial distribution $W_0(q,p)$, which according to the uncertainty principle is restricted by the inequalities (11) or (17) so as to exclude delta-function wave packets which would correspond to the initial simultaneous specification of q and p. Spreading is then simply a consequence of the mapping apart of

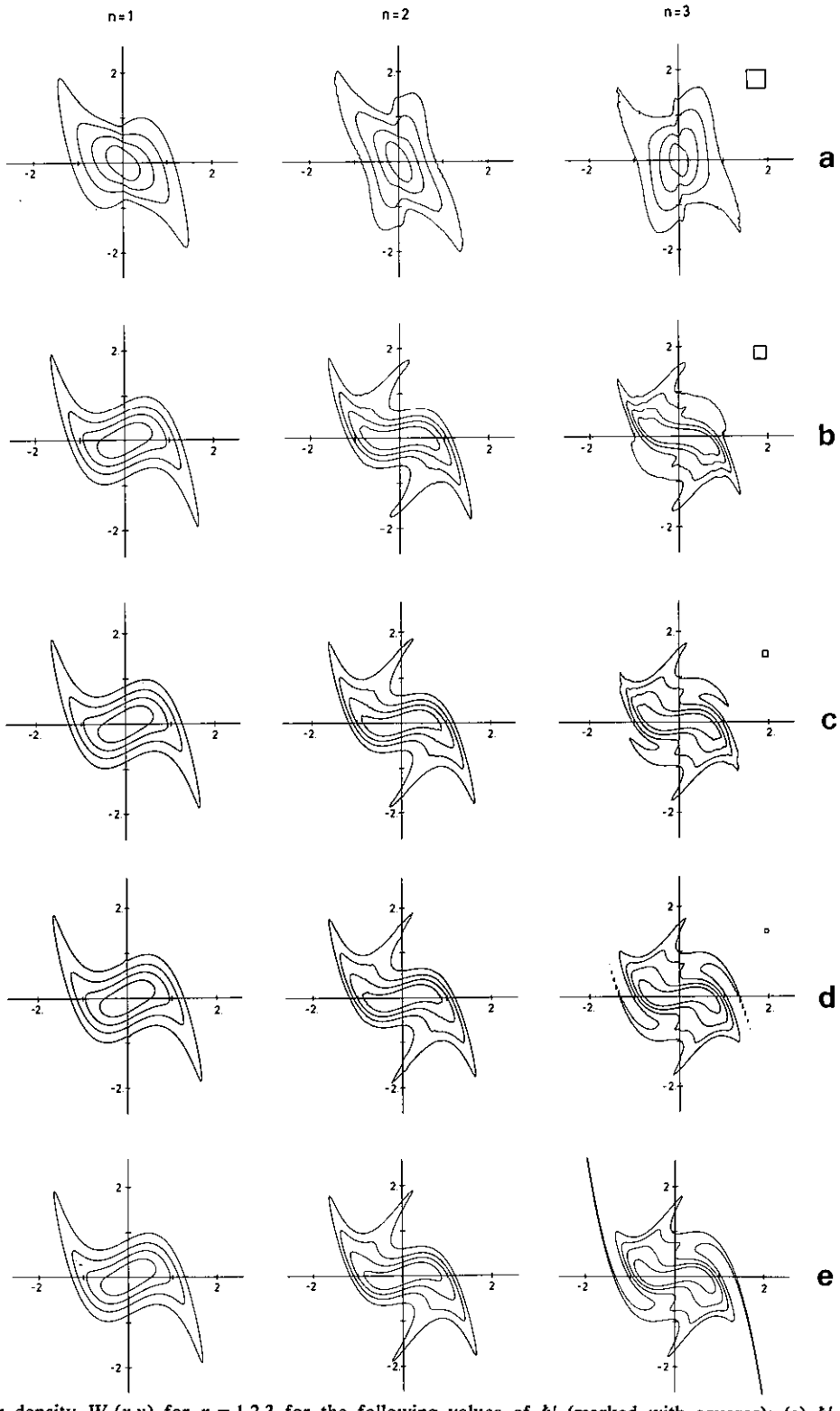

Fig. 4. Wigner density $W_n(x,y)$ for $n = 1,2,3$ for the following values of $\hbar'$ (marked with squares): (a) $\hbar' = 0.5$ (extreme quantum-mechanical case); (b) $\hbar' = 0.1$; (c) $\hbar' = 0.02$; (d) $\hbar' = 0.01$; (e) $\hbar' = 0$ (classical limit). The initial distribution is the same as in figs. 1–3.

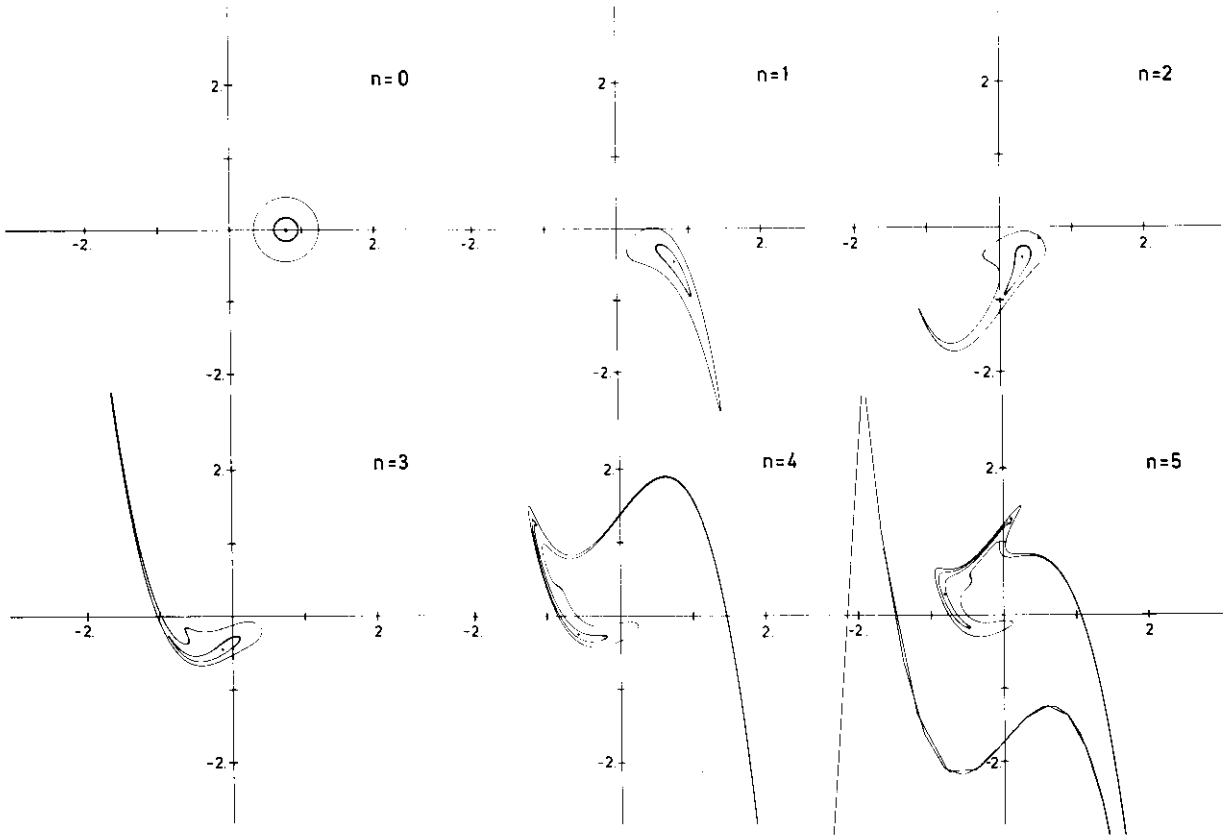

Fig. 5. Classical mapping of an initial Gaussian phase-space density with $\Delta = 0.25$ centered in the chaotic region at $\bar{x} = 0.78$, $\bar{y} = 0$, for $n = 0,1,2,3,4,5$. The contour lines are drawn for 80% and 20% of the maximum, whose positions are marked with a dot.

different momenta in the original packet. Likewise, the spreading is purely classical if $V(q)$ is linear or quadratic. But if the non-linearity of $V(q)$ is worse than quadratic, and in particular if $V(q)$ is quartic as in our computations, then not only is the classical spreading now much faster because of the chaotic shooting-out of tendrils, but also the quantum-mechanical spreading is nonclassical because of the nonlocal character of the propagator (13). This nonlocality, explicit in (15), implies that any W_0 will map into a W_n with nonzero values at arbitrarily large q and p, even after a single iteration. Despite this, it appears from our computations that the bulk of the quantum-mechanical Wigner function spreads more slowly than the classical distribution.

Of course our computations are suggestive rather than conclusive, and it is desirable to have analytical understanding of behaviour of maps such as (15) under repeated iteration. The simplest calculation would appear to be a study of the evolution of the variance in q and p of W_n as $n \to \infty$, but even this seems very difficult.

Finally, we remark on the similarity of some of our contour plots to pictures computed by Zabusky and his collaborators [11, 12] in the quite different context of the evolution of fluid vorticity distributions under two-dimensional incompressible nearly-inviscid flow. Incompressibility implies that the fluid motion is a continuously-evolving area-preserving map of points in the plane (fluid particles). If in addition the viscosity is zero, then the fluid particles retain their vorticity, and vorticity contours map so as to preserve their area, just

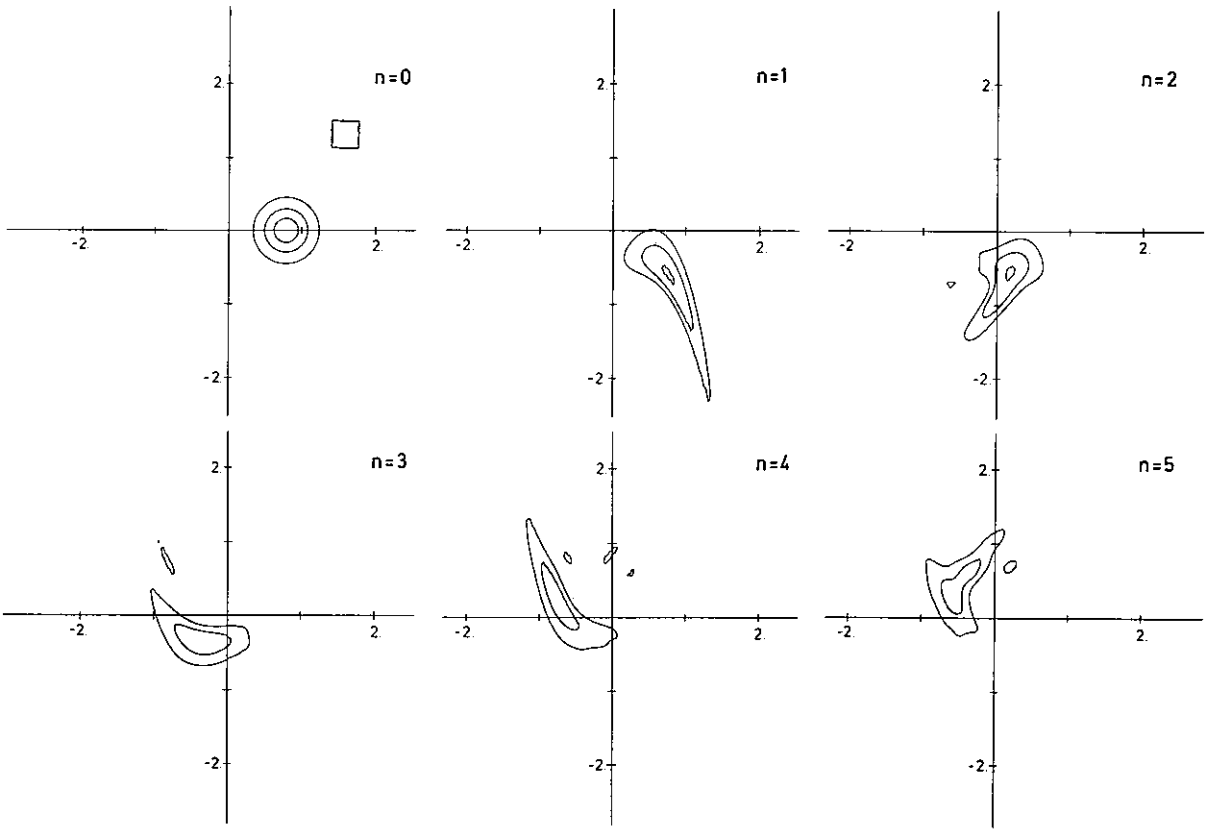

Fig. 6. Quantum mapping of the Wigner density $W_n(x,y)$ for $n = 0,1,2,3,4,5$. The initial distribution is the same as in fig. 5. $\hbar' = 1/8$ (extreme quantum-mechanical case) and a square of this area is drawn on the $n = 0$ picture.

like classical Wigner-function contours under the Liouville mapping. Unlike the Liouville mapping, however, each point evolves in a way that depends convectively on the whole vorticity distribution, rather than being imposed by the 'external' potential $V(q)$. Despite this, vorticity contours can develop an arbitrary complexity of the 'whorl-and-tendril' type that we see in our classical Wigner plots, corresponding to the turbulence-like morphologies displayed by cream on the surface of coffee. The introduction of a small amount of viscosity prevents the development of fine structure in the vorticity contours, on account of the 'nonlocal' diffusion of vorticity away from the fluid particles to which it was previously attached. In this respect Zabusky [11, 12] finds viscosity to have a smoothing effect analogous to what we describe here for Planck's constant. In other respects, of course, the quantum-mechanical and fluid dynamics are very different.

Acknowledgments

H.J.K. thanks the U.K. Science Research Council for financial and computational support. M.V.B. thanks the Institute for Theoretical Physics, Utrecht for hospitality whilst this paper was written. This work was not supported by any military agency.

References

[1] M.V. Berry, N.L. Balazs, M. Tabor and A. Voros, Ann. Phys. (N.Y.) 122 (1979) 26.

[2] E.P. Wigner, Phys Rev. 40 (1932) 749.
[3] H.J. Groenewold, Physica 12 (1946) 405.
[4] J.E. Moyal, Proc. Camb. Phil. Soc. 45 (1949) 99.
[5] T. Takabayasi, Progr. Theor. Phys. Japan 11 (1954) 341.
[6] G.A. Baker Jr., Phys. Rev. 109 (1958) 2198.
[7] M.V. Berry, Phil. Trans. Roy. Soc. London A287 (1977) 237.
[8] G. Casati, B.V. Chirikov, F.M. Izraelev and J. Ford, in: Stochastic Behaviour in Classical and Quantum Hamiltonian Systems, G. Casati and J. Ford, eds., Springer Lecture notes in physics No 93 (1979) p. 334.
[9] M. Abramowitz and I.A. Stegun, Handbook of Mathematical Functions (U.S. National Bureau of Standards, Washington, DC 1964).
[10] M.V. Berry, Singularities in Waves and Rays, to be published in the Les Houches lecture notes for 1980, M. Kléman and J.-P. Poirier, eds. (North-Holland, Amsterdam).
[11] N.J. Zabusky, M.H. Hughes and K.V. Roberts, J. Comput. Phys. 30 (1979) 96.
[12] N.J. Zabusky, Coherent structures in fluid dynamics in Proc. Orbis Scientiae (Miami) on the Significance of Nonlinearity in the Natural Sciences, A. Perlmutter and L.F. Scott, eds. (Plenum, New York, 1977) p. 145.
[13] J.S. Hutchinson and R.E. Wyatt, Chem. Phys. Lett. 72 (1980) 378.